EFFICIENT OPTIMIZATION DESIGN METHOD USING KRIGING MODEL

Shinkyu Jeong[1], Mitsuhiro Murayama[2]
and
Kazuomi Yamamoto[3]

Information Technology Center,
Institute of Space Technology and Aeronautics
Japan Aerospace Exploration Agency, *Chofu, Tokyo, 182-8522, Japan*

Abstract

The Kriging-based genetic algorithm is applied to aerodynamic design problems. The Kriging model, one of the response surface models, represents a relationship between the objective function (output) and design variables (input) using stochastic process. The kriging model drastically reduces the computational time required for objective function evaluation in the optimization (optimum searching) process. 'Expected improvement (EI)' is used as a criterion to select additional sample points. This makes it possible not only to improve the accuracy of the response surface but also to explore the global optimum efficiently. The functional analysis of variance (ANOVA) is conducted to evaluate the influence of each design variable and their interactions to the objective function. Based on the result of the functional ANOVA, designers can reduce the number of design variables by eliminating those that have small effect on the objective function. In this paper, the present method is applied to a two-dimensional airfoil design and the prediction of flap's position in a multi-element airfoil, where the lift-to-drag ratio (L/D) is maximized.

1. Introduction

With the growth in computing power of current computers and the advance in technique of computational fluid dynamics (CFD), CFD becomes one of the inevitable tools in the aerodynamic optimization design nowadays. However, in the process of the optimization design, the number of objective function evaluations using high fidelity CFD analysis solver is severely limited by time and cost, even with the current supercomputer.

One alternative is to construct a simple approximate model of the complicated CFD analysis solver. The approximate model expresses the relationship between the objective function (output) and the design variables (input) with simple equation. This model requires very little time to evaluate the objective function. It makes possible to save a lot of computation time and to explore more wide design space.

The most widely used approximation model is polynomial-based model [1, 2], due to its simplicity and ease of use. However, this model is not suitable for representing multi-modalities and non-linearity that often appear in the aerodynamic problem.

Recently, the Kriging model [3, 4], developed in the field of spatial statistics and geostatistics, has gained popularity in this field. This model predicts the value of the unknown point using stochastic processes. Sample points are interpolated with the Gaussian random function to estimate the trend of the stochastic processes. The model has a sufficient flexibility to represent the nonlinear and multimodal functions at the expense of computation time. However, the computation time to construct the Kriging model is still short compared to that of the direct CFD analysis.

In this study, the genetic algorithms (GAs) are adopted as searching algorithm. GAs are based on the mechanism of natural selection and natural genes. GAs are very attractive to the engineering problems where discontinuities and multi-modalities may exist, because GAs do not utilize derivative information. Another merit of GAs is that they search the optimum point from a population of points, not a single point. This feature is very promising to multi-objective problems. However, GAs require many objective function evaluations, which may be impractical if we rely solely on the time-consuming high fidelity CFD analysis solver.
The time consuming CFD analysis solver in the objective function evaluation process of GA is replaced with the Kriging model. However, it is possible to miss the global optimum in the searching space if we rely only on the prediction value of the Kriging model, because the model includes uncertainty at the prediction point. For the robust exploration of the global optimum point, both the prediction value and its uncertainty should be considered at the same time. This concept is expressed in the criterion 'expected improvement (EI)'. EI indicates the probability of a point being optimum in the design space.

1. Invited researcher
2. Scientist, AIAA member
3. Senior researcher, AIAA member

By selecting the best EI point as the additional sample point, the improvement of the model and the robust exploration of the global optimum can be achieved at the same time.

Current optimization design problem treats a lot of design variables. Sometime the number of design variable is more than several hundreds. In this study, a variance decomposition of the model, using a functional analysis of variance (ANOVA) [5, 6, 7], is employed to evaluate the effect of each variable and their interactions to the objective function. Based on these results, design variable that does not have a significant influence to the objective function can be eliminated effectively.

2. Kriging Model

The present Kriging model expresses the unknown function y(**x**) as

$$y(\mathbf{x}) = \mu + Z(\mathbf{x}) \tag{1}$$

where $\mathbf{x}$ is an m-dimensional vector (m design variables), μ is a constant global model and $Z(\mathbf{x})$ represents a local deviation from the global model. In the model, the local deviation at an unknown point ($\mathbf{x}$) is expressed using stochastic processes. The sample points are interpolated with the Gaussian random function as the correlation function to estimate the trend of the stochastic processes. The correlation between $Z(\mathbf{x}^i)$ and $Z(\mathbf{x}^j)$ is strongly related to the distance between the two corresponding points, $\mathbf{x}^i$ and $\mathbf{x}^j$. However, the Euclidean distance is not used, because it weighs all design variables equally. In the Kriging model, a special weighted distance is used instead.
The distance function between the point at $\mathbf{x}^i$ and $\mathbf{x}^j$ is expressed as

$$d(\mathbf{x}^i, \mathbf{x}^j) = \sum_{k=1}^{m} \theta_k \left| x_k^i - x_k^j \right|^2 \tag{2}$$

where θ_k $(0 \le \theta_k \le \infty)$ is the k_{th} element of the correlation vector parameter $\boldsymbol{\theta}$. By using the specially weighted distance and the Gaussian random function, the correlation between the point $\mathbf{x}^i$ and $\mathbf{x}^j$ is defined as

$$Corr\left[Z(\mathbf{x}^i), Z(\mathbf{x}^j)\right] = \exp\left[-d(\mathbf{x}^i, \mathbf{x}^j)\right] \tag{3}$$

The Kriging predictor is

$$\hat{y}(\mathbf{x}) = \hat{\mu} + \mathbf{r}'\mathbf{R}^{-1}(\mathbf{y} - \mathbf{1}\hat{\mu}) \tag{4}$$

where $\hat{\mu}$ is the estimated value of μ, $\mathbf{R}$ denotes the $n \times n$ matrix whose (i, j) entry is $Corr\left[Z(\mathbf{x}^i), Z(\mathbf{x}^j)\right]$. $\mathbf{r}$ is vector whose i_{th} element is

$$r_i(\mathbf{x}) \equiv Corr\left[Z(\mathbf{x}), Z(\mathbf{x}^i)\right] \tag{5}$$

and $\mathbf{y} = [y(x^1), ..., y(x^n)]$.

The detailed derivation of Eq. (4) can be found in [8].

The unknown parameter to be estimated for constructing the Kriging model is $\boldsymbol{\theta}$. This parameter can be estimated by maximizing the following likelihood function

$$\begin{aligned} Ln(\hat{\mu}, \hat{\sigma}^2, \boldsymbol{\theta}) = &-\frac{n}{2}\ln(2\pi) - \frac{n}{2}\ln(\hat{\sigma}^2) - \frac{1}{2}\ln\left(|\mathbf{R}|\right) \\ &- \frac{1}{2\hat{\sigma}^2}(\mathbf{y} - \mathbf{1}\hat{\mu})' \mathbf{R}^{-1}(\mathbf{y} - \mathbf{1}\hat{\mu}) \end{aligned} \tag{6}$$

where **1** denotes an m-dimensional unit vector.

Maximizing the likelihood function is an m-dimensional unconstrained non-linear optimization problem. In this paper, the alternative method [9, 10] is adopted to solve this problem.

For a given $\boldsymbol{\theta}$, $\hat{\mu}$ and $\hat{\sigma}^2$ can be defined as

$$\hat{\mu} = \frac{\mathbf{1}'\mathbf{R}^{-1}\mathbf{y}}{\mathbf{1}'\mathbf{R}^{-1}\mathbf{1}} \tag{7}$$

$$\hat{\sigma}^2 = \frac{(\mathbf{y} - \mathbf{1}\mu)' \mathbf{R}^{-1}(\mathbf{y} - \mathbf{1}\mu)}{n} \tag{8}$$

Next, vector $\boldsymbol{\theta}$ is updated by using

$$\boldsymbol{\theta}^{new} = \boldsymbol{\theta}^{old} + \mathbf{B}^{-1}\frac{\partial Ln}{\partial \boldsymbol{\theta}} \tag{9}$$

where

$$\begin{aligned} \frac{\partial Ln}{\partial \theta_k} = &-\frac{1}{2} tr\left\{ \frac{1}{\mathbf{R}} \frac{\partial \mathbf{R}}{\partial \theta_k} \right\} \\ &- \frac{1}{2\sigma^2}(\mathbf{y} - \mathbf{1}\mu)' \frac{1}{\mathbf{R}} \frac{\partial \mathbf{R}}{\partial \theta_k} \frac{1}{\mathbf{R}} (\mathbf{y} - \mathbf{1}\mu) \end{aligned} \tag{10}$$

and the $(i, j)_{\text{th}}$ element of matrix $\mathbf{B}$ is $\frac{1}{2} t_{ij}$ with

$$t_{ij} = tr(\mathbf{R}^{-1} \frac{\partial \mathbf{R}}{\partial \theta_i} \mathbf{R}^{-1} \frac{\partial \mathbf{R}}{\partial \theta_j}). \tag{11}$$

For this updated $\boldsymbol{\theta}^{new}$, new values of $\hat{\mu}$ and $\hat{\sigma}^2$ can be calculated using Eq. (7) and (8). This routine is iterated until function Ln converges to a maximum value.

The accuracy of the prediction value largely depends on the distance from sample points. Intuitively speaking, the closer point $\mathbf{x}$ to sample points, the more accurate is the prediction $\hat{y}(\mathbf{x})$. This intuition is expressed in following Equation.

$$s^2(\mathbf{x}) = \hat{\sigma}^2 \left[1 - \mathbf{r}'\mathbf{R}^{-1}\mathbf{r} + \frac{(1 - \mathbf{1}\mathbf{R}^{-1}\mathbf{r})^2}{\mathbf{1}'\mathbf{R}^{-1}\mathbf{1}} \right] \tag{12}$$

$s^2(\mathbf{x})$ is the mean squared error of the predictor. $s(\mathbf{x})$ indicates the uncertainty at the estimation point. The root mean squared error (RSME) is expressed as $s = \sqrt{s^2(\mathbf{x})}$.

3. Genetic algorithms (GAs) as optimizer

Genetic algorithms (GAs) [11] are a searching

mechanism based on natural selection and genetics. GAs use the objective function value itself, not its derivative information. This feature makes GAs robust and attractive to the aerodynamic design problems where non-linearity, multi-modality and discontinuities may exist. Another merit of GAs is that they search the optimum point from a population of points, not a single point. It makes GAs the promising methods for the multi-objective (MO) problems. The population of points can represent Pareto optimal set of MO problems [12]. The definition of Pareto optimality is as follow:

Suppose $X_1 = (x_1, y_1)$ and $X_2 = (x_2, y_2)$ are in the population and $F = (f_1, f_2)$ is the set of objective functions to be maximized

1. X_1 is said to be dominated by X_2, if $F(X_1)$ is partially less than $F(X_2)$, i.e., $f_1(X_1) \le f_1(X_2) \cap f_2(X_1) \le f_2(X_2)$ and $F(X_1) \ne F(X_2)$.
2. X_1 is said to be non-dominated if there doesn't exist X_2 in the population that dominates X_1.

In Figure 1, red points are the Pareto solutions. Each point in the Pareto set is optimal in the sense that no improvement can be achieved in any objective function without degradation in the others.

The general procedure of the genetic algorithms is shown in Figure 2.

1. Creation of initial population
2. Evaluation of fitness (objective) function
3. Selection of parents according to the rank (fitness)
4. Crossover and mutation
5. Check the convergence. If not converged, the algorithm returns to the process No. 2.

4. Exploration of the global optimization and improvement of the model

Once the approximation model is constructed, the optimum point can be explored using an arbitrary optimizer on the model. However, it is possible to miss the global optimum, because the approximation model includes uncertainty at the predicted point.

In Figure 3, the solid line is the real shape of objective function. Eight points are selected for constructing the Kriging model and the dots line represents the predicted value by the Kriging model. The minimum point on the Kriging model is located near x=9, whereas, the real global minimum of the objective function is sited near x=4. However hard we search the global minimum on the present Kriging model, the real global minimum near x=4 cannot be found. For a robust search of the global optimum, the predicted value by the Kriging model and its uncertainty should be considered at the same time.
Figure 4 shows the predicted value and the standard error of the Kriging model. Around x=9.5, the standard error of the Kriging model is very small because there are many sample points around this point. Thus, the confidence interval is very short as shown in Figure 4.
On the other hand, the standard error is very large around x=3.5 due to the lack of sample points around there. Thus, the confidence interval at this point is very wide. The minimum inside this interval is less than the present minimum point on the Kriging model. This point has a somewhat large probability to become the global minimum.

This concept is expressed in the criterion of EI [10]. The EI of minimization problem can be calculated as follows

$$E[I(\mathbf{x})] = (f_{\min} - \hat{y})\Phi\left(\frac{f_{\min} - \hat{y}}{s}\right) + s\phi\left(\frac{f_{\min} - \hat{y}}{s}\right) \quad (13)$$

where $f_{\min}$ is the minimum value among n sampled values. Φ and ϕ are the standard distribution and normal density, respectively. By selecting the maximum EI value point as an additional sample point, the robust exploration of the global optimum and the improvement of model can be achieved simultaneously.

5. Visualization of model

One of the advantages of using approximation model is that it shows the relationship between the objective function and design variables. This relationship is very helpful to identify how much influence each design variable has on the objective function. Based on the result, designer can eliminate the design variables that do not have significant effect on objective function. In order to evaluate the effect of each design variable, the total variance of the model is decomposed into that of each design variable and their interactions. It is called the functional analysis of variance (ANOVA). The decomposition is accomplished by integrating variables out of the model $\hat{y}$. The total mean $(\hat{\mu}_{total})$ and variance $(\hat{\sigma}^2_{total})$ of model $\hat{y}$ are as follows:

$$\hat{\mu}_{total} \equiv \int \cdots \int \hat{y}(x_1, ..., x_n) dx_1 \cdots dx_n \quad (14)$$

$$\hat{\sigma}^2_{total} = \int \cdots \int [\hat{y}(x_1, ..., x_n) - \hat{\mu}]^2 dx_1 \cdots dx_n \quad (15)$$

The main effect of variable x_i is

$$\hat{\mu}_i(x_i) \equiv \int \cdots \int \hat{y}(x_1, \cdots, x_n) dx_1 \cdot\cdot dx_{i-1} dx_{i+1} \cdot\cdot dx_n - \hat{\mu} \quad (16)$$

The two-way interaction effect of variable x_i and x_j is

$$\hat{\mu}_{i,j}(x_i, x_j) \equiv \int \cdots \int \hat{y}(x_1, ..., x_n) dx_1 \cdot\cdot dx_{i-1} dx_{i+1} \cdot\cdot dx_{j-1} dx_{j+1} \cdot\cdot dx_n - \hat{\mu}_i(x_i) - \hat{\mu}_j(x_j) - \hat{\mu} \quad (17)$$

$\hat{\mu}_i(x_i)$ and $\hat{\mu}_{i,j}(x_i, x_j)$ quantify the effect of variable x_i and interaction effect of x_i and x_j on the objective function.

The variance due to the design variable x_i is

$$\int [\hat{\mu}_i(x_i)]^2 dx_i \tag{18}$$

The proportion of the variance due to design variable x_i to total variance of model can be expressed by dividing Eq. (18) with Eq. (15).

$$\frac{\int [\hat{\mu}_i(x_i)]^2 dx_i}{\int \cdots \int [\hat{y}(x_1, \ldots\ldots, x_n) - \hat{\mu}]^2 dx_1 \cdots dx_n} \tag{19}$$

This value indicates the sensitivity of the objective function to the variation of the design variables and their interactions.

6. Results

In this study, the Kriging-based genetic algorithm was applied to a two-dimensional airfoil design and the optimization of a flap's position in a multi-element airfoil to maximize the lift-to-drag ratio (L/D).

1) Airfoil design

The first design problem is to maximize L/D of an airfoil at the condition of Mach=2.0 and an angle of attack (AOA) =2.0°, under the constraint of maintaining the cross-sectional area of the airfoil to the same level of RAE2822.

Definition of airfoil geometry and design variable

The geometry was parameterized by the PARSEC airfoil [13]. This parameterization technique was developed to keep the number of design variable as low as possible while controlling important transonic aerodynamic features effectively. Figure 5 illustrates 11 basic parameters for PARSEC airfoil:

1. Leading edge radius (r_{LE})
2. Trailing-edge coordinate (Z_{TE})
3. Trailing-edge direction (α_{TE})
4. Trailing-edge wedge angle (β_{TE})
5. The crest of upper surface's X coordinate (X_{UP})
6. The crest of upper surface's Z coordinate (Z_{UP})
7. The curvature at the crest of upper surface (Z_{XXUP})
8. The crest of lower surface's X coordinate (X_{LO})
9. The crest of lower surface's Z coordinate (Z_{LO})
10. The curvature at the crest of lower surface (Z_{XXLO})
11. The trailing edge thickness (ΔZ_{TE})

In this study, only sharp trailing-edge airfoil was considered, therefore ΔZ_{TE} was set to zero. A total of 10 design variables were used to define the geometry of airfoil.

Design space and selection of sample points

The upper and lower bound of each parameter was determined lest the PARSEC should reproduce unrealistic airfoil geometry such as fish-tailed airfoil. The parameter ranges of design space are shown in Table 1.

Table 1. Parameter ranges of design space

	Lower bound	Upper bound
r_{LE}	0.005	0.06
X_{UP}	0.35	0.50
Z_{UP}	0.05	0.15
X_{LO}	0.35	0.50
Z_{LO}	-0.12	-0.04
Z_{XXUP}	-1.0	-0.4
Z_{XXLO}	0.3	1.0
Z_{TE}	-0.02	0.02
α_{TE}	-8°	-3°
β_{TE}	4°	8°

In this design space, the sample points were selected by using the orthogonal arrays (OAs) [6, 7]. OAs has a good property of distributing points in multi-dimensional design space uniformly. Important parameters of OAs are *strength* and *level*. If the OAs has *strength k* and *level l*, all projections to *k*-dimension are uniformly distributed. The OAs used in this investigation has *strength* 2 and *level* 5 with 50 sample points. Figure 6 shows geometry of some sample airfoils. The OAs code used in this study was downloaded from STATLIB (http://lib.stat.cmu.edu).

Genetic algorithm with the Kriging model

The performance of 50 sample airfoils was evaluated using a Navier-Stokes code. This code utilized a TVD upwind scheme for spatial discretization of convective terms and a LU-SGS method [14] for time integration. A Kriging model was then constructed based on the sample data and the model was used for the objective function evaluation in the optimization process of GA. However, if GA searches the maximum L/D point based only on the predicted value by Kriging model, it may miss the global maximum point because the model has some uncertainty at the predicted point. In this study, the objective function L/D was transformed to the EI to find the global optimum point robustly and the design constraint was treated as the other objective function of the optimization problem.

Thus, the single objective problem, '*the maximization of L/D'*, is thus changed to the MO problem, '*the maximization of both EI and Area ratio'*. The objective functions are expressed as follows:

$$E[I(\mathbf{x})] = (\hat{y} - L/D_{\max})\Phi\left(\frac{\hat{y} - L/D_{\max}}{s}\right) + s\phi\left(\frac{\hat{y} - L/D_{\max}}{s}\right) \tag{20}$$

$$Area\ ratio = 1. - \frac{abs(A - A_{rae2822})}{A_{rae2822}} \tag{21}$$

A: cross-section area of airfoil,

A_{RAE2822}: cross-section area of RAE2822 airfoil

This MO problem was solved by Multi-objective

genetics algorithm (MOGA). The number of both population and generation are 100. The Pareto set obtained by MOGA is shown in the Figure 7. Among the Pareto solutions, the airfoil that shows the highest L/D performance was selected as additional sample one. Then, the performance of the airfoil was evaluated by the Navier-Stokes code and the Kriging model was updated with 51 sampled data. This routine was iterated until L/D was not improved any more. After 5 additional sample airfoil selections, there was no L/D improvement. The geometry and pressure distribution of the optimized airfoil are shown in Figure 8. The L/D performance and the cross-section area of optimized airfoil are compared with those of RAE2822 in Table 2. L/D is improved within the design constraint.

Table 2. Comparison of L/D and section area of airfoils

	L/D	Area of Cross-section
RAE2822	58.0178	0.07777
Optimum	60.7546	0.07864

Functional analysis of variance (ANOVA)

In order to estimate the main and the two-way interactions effect of design variables, the total variance of model was decomposed into that of each design variable and their interactions. Figure 9 shows the main effect of design variables. According to the main effect plot, the objective function (L/D) is sensitive to the change of Z_{LO}, Z_{UP}, r_{LE}, Z_{XXUP} and Z_{XXLO} and is insensitive to the change of other design variables.

There are 45 two-way interactions because the number of design variable is 10. Two of those two-way interactions are plotted in Figure 10. According to the result, the objective function is sensitive to the change of the interaction Z_{UP}-Z_{LO} and is insensitive to the change of the interaction r_{LE}- Z_{XXUP}.

The proportion of the variance due to the each design variable and their interactions to the total variance was calculated by using Eq. (19). Design variables and their interactions whose proportion to total variance is over than 1.0% are shown in Figure 11.

According to these results, it seems that Z_{LO}, Z_{UP}, r_{LE}, Z_{XXUP}, Z_{XXLO} are very important variables in L/D optimization design. On the other hand, other parameters seem less important to the design of high L/D airfoil.

Design of airfoil using 5 variables

In order to verify the result of the functional ANOVA, airfoil design was performed with only 5 important design variables (Z_{LO}, Z_{UP}, r_{LE}, Z_{XXUP}, Z_{XXLO}). The geometry and pressure distribution of the optimized airfoil with 5 design variables are compared with those of the optimized airfoil with 10 design variables and RAE2822 in Figure 12. The geometry near the trailing edge show a somewhat large difference between the design result of 5-variable and 10-variable case, because the design variables defining the shape near the trailing edge are fixed in 5-variable case. The L/D performance and cross-sectional area of the airfoil designed with 5 variables are also compared with those of the airfoil designed with 10 variables and RAE2822, in Table 3. The L/D of the 5-variable case is slightly less than that of the 10-variable case, however, it is still larger than that of RAE2822, while satisfying the design constraint. It shows the validity of the eliminating the design variable that has little influence on the objective function based on the result of the functional ANOVA.

Table 3. Comparison of L/D and cross-sectional area of airfoils

	L/D	Area of cross-section
RAE2822	58.0178	7.7777e-02
Design-10	60.7546	7.8637e-02
Design-5	60.1225	7.7997e-02

For the case of 5 design variables, the functional ANOVA was also performed. Figure 13 shows the proportion of variance due to the each design variable and their interactions to the total variance of model. According to the result, Z_{UP}, r_{LE}-Z_{UP}, Z_{LO} and Z_{XXUP} have a large influence to L/D

2) Optimization of flap's position

The second optimization problem is to find the position of the flap where the L/D of multi-element airfoil is maximized at a specified flow condition (Mach=0.185, AOA=6°, Re=2.51×10^6).

The geometry and design space

The multi elements airfoil used in the study is NLR7301 [15] with single flap of 32% chord. The position of flap is defined by three parameters (x_F/c, y_F/c, δ_F), as shown in Figure 14.

The parameter ranges of design space is defined as follows:

$$-5\% \le x_F / c \le 10\%$$

$$2\% \le y_F / c \le 10\%$$

$$0° \le \delta_F \le 40°$$

Selection of sample points and evaluation

25 sample points were selected using OAs of *strength* 5 and *level* 2. The evaluations of sample points are performed using TAS code (Tohoku University Aerodynamic Simulation code) that is composed of unstructured mesh generator (TAS_MESH) [16, 17] and flow solver (TAS_FLOW). Figure 15 shows the computational mesh around the multi-element airfoil generated by TAS_MESH. The prisms layers are located near the wall for the viscous flows.

The flow solver, TAS_FLOW, is a Navier-Stokes code, which uses a finite volume cell-vertex scheme. The HLLEW (Haren-Lax-van Leer-Einfeldt-Wada Riemann

solver) is used for the numerical flux calculation and the LU-SGS method [14] is used for time integration. The Spalart-Allmaras model [18] is implemented to treat turbulent layer.

Genetic algorithm with Kriging model

The performance of 25 sample points was evaluated using TAS code and then the Kriging model was constructed based on these sampled data. The Kriging model was utilized for the objective function evaluation in the process of GA. Instead of searching for the maximum L/D point on the Kriging model directly, GA searches for the maximum EI point on the Kriging model to improve the robustness in finding the global optimum point. The predicted optimum position of flap is x_F/c = 1.82, y_F/c = 5.78, δ_F=9.66° and the L/D at that position was 86.2. Figure 16 shows the L/D plots (at δ_F=9.66°) predicted by the Kriging model. According to the plot, x_F/c did not give a significant effect to the L/D of the multi-element airfoil, NLR7301.

Conclusion

In this study, the Genetic algorithm using the Kriging model for objective function evaluation was introduced. The Kriging model, one of the response surface models, represents a relationship between the objective function (output) and design variables (input) using stochastic process. Replacing the CFD analysis solver with the Kriging model drastically reduced the computational time required for the objective function evaluation. A criterion 'expected improvement (EI)' was used for the selection of the additional sample point. This made it possible not only to improve the accuracy of the response surface but also to explore the global optimum efficiently. The functional analysis of variance (ANOVA) was conducted to evaluate the effect of each design variable and their interactions to the objective function. It was very helpful to reduction of the number of design variable. The present method was applied to a two-dimensional airfoil design and the prediction of flap's position where the lift-to-drag ratio (L/D) of a two-element airfoil is maximized. The result confirmed the validity of the present method.

Reference

1. Myers, R. H. and Montgomery, D. C, *Response Surface Methodology*: Process and Product Optimization Using Designed Experiments, John Wiley & Sons, New York, 1995.
2. Chen, W., Allen, J. K., Schrage, D. P., and Mistree, F., "Statistical Experimentation Methods for Achieving Affordable Concurrent Systems Design," *AIAA Journal*, Vol. 35, No. 5, pp. 892-900, 1997.
3. Timothy, W. S., Timothy M. M., John, J. K. and Farrokh, M, "Comparison of Response Surface And Kriging Models for Multidisciplinary Design Optimization," AIAA paper 98-4755.
4. Anthony A. G. and Layne T. W., "A Comparison of Approximation Modeling Techniques: Polynomial Versus Interpolating Models," AIAA paper 98-4758.
5. Sack, J., Welch, W. J., Mitchell, T. J. and Wynn, H. P., "Design and analysis of computer experiments (with discussion)," Statistical Science 4, pp. 409-435, 1989.
6. Booker, A. J., "Design and analysis of computer experiments," AIAA paper 98-4757.
7. Owen, A. B., "Orthogonal arrays for computer experiments, integration and visualization," *Statistica Sinica*, Vol. 2, pp. 439-452, 1992.
8. Koehler, J and Owen, A. Computer experiments, in S. Ghosh and C. R. Rao (eds.), *Handbook of Statistics*, 13: *Design and Analysis of Experiments*, pp. 261-308, Elsevier, Amsterdam, 1996.
9. Mardia, K. V. and R. J. Marshall, "Maximum likelihood estimation of models for residual covariance in Spatial regression," *Biometrika* Vol. 71, pp. 135-146, 1984.
10. Donald, R. J., Matthias S and William J. W, "Efficient Global Optimization of Expensive Black-Box Function," *Journal of global optimization*, Vol. 13, pp. 455-492, 1998.
11. Goldberg, D. E., "Genetic Algorithms in Search, Optimization & Machine Learning," Addison-Wesley Publishing, Inc., Reading, Jan., 1989.
12. Takami, H., Kita, H., and Kobayashi, S., "Multi-Objective Optimization by Genetic Algorithms: A Review," Proceedings of 1996 IEEE International Conference on Evolutionary Computation, pp. 517-522, 1996.
13. Sobieczky, H., "Parametric Airfoils and Wings, Recent Development of Aerodynamic Design Methodologies-Inverse Design and Optimization-," Friedr. Vieweg & Sohn Verlagsgesellschaft mbH, Braunschweig/Wiesbaden, Germany, pp. 72-74, 1999.
14. Obayashi, S. and Guruswamy, G. P., "Convergence Acceleration of a Aeroelastic Navier-Stokes Solver," *AIAA Journal*, Vol. 33, No. 6, pp. 1134-1141, 1995.
15. Van der Berg, B., "Boundary layer measurements on a two-dimensional wing with flap," NLR TR 79009 U, 1979.
16. Sharov, D. and Nakahashi, K., "A boundary Recovery Algorithm for Delaunay Tetrahedral Meshing," Proceedings of 5th International Conference on Numerical Grid Generation on Computational Field Simulations, 1996, pp. 229-238.
17. Ito, Y. and Nakahashi, K., "Unstructured Mesh Generation for Viscous Flow Computations," Proceedings of the 11th International Meshing Roundtable, Ithaca, NY, Sept. 2002, pp. 367-376.
18. Fares, E., Meinke, M. and Schöder, W., "Numerical Engine Jets in the Near Field," AIAA paper 2000-2222, 2000.

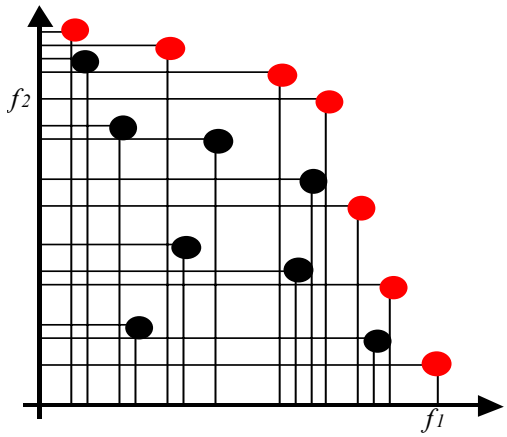

Figure 1. Pareto set of MO problem

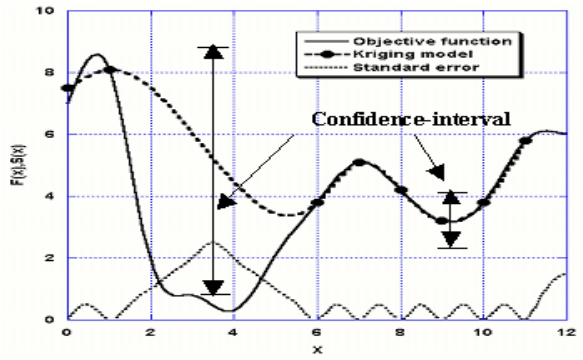

Figure 4. The predicted value and the standard error of the Kriging model

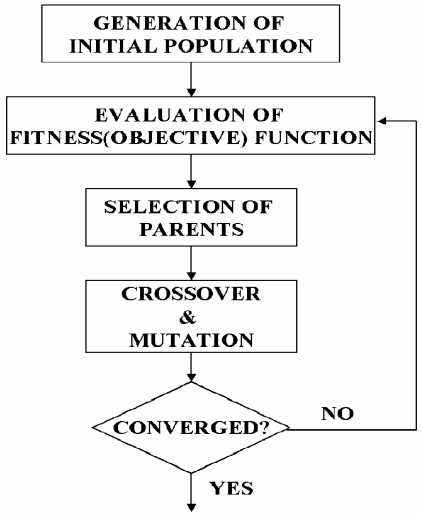

Figure 2. Flow chart of Genetic Algorithms

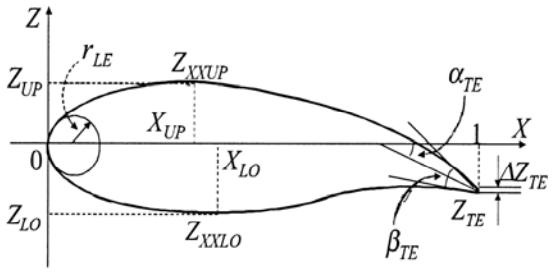

Figure 5. PARSEC airfoil and its parameters

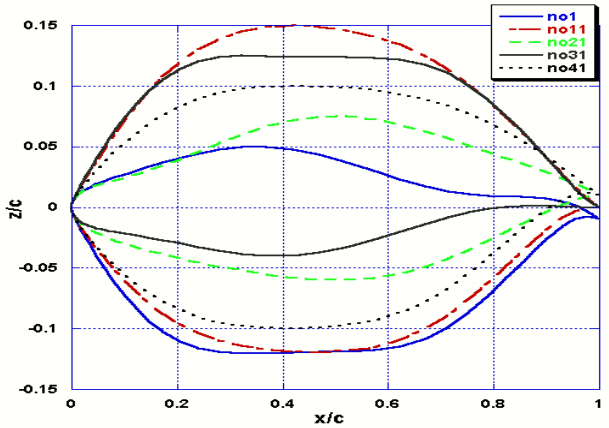

Figure 6. Geometry of some sample airfoils

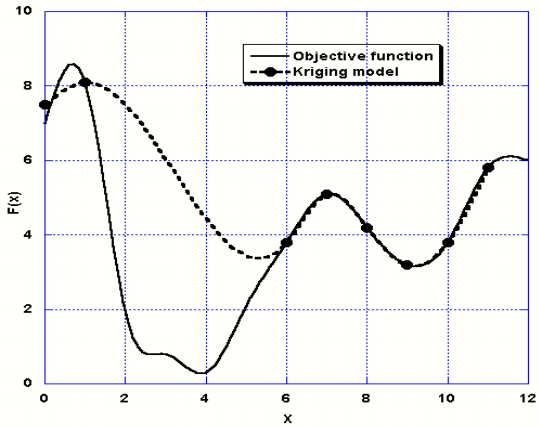

Figure 3. The objective function and the Kriging model

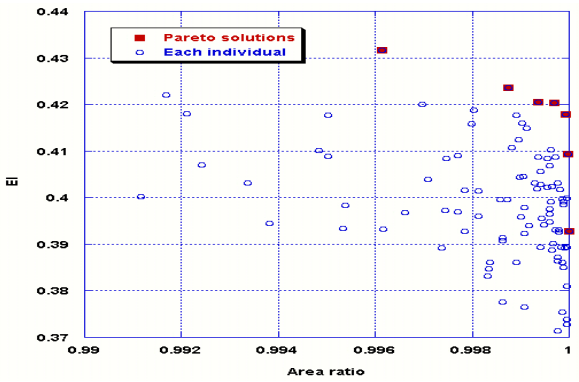

Figure 7. The Pareto solutions

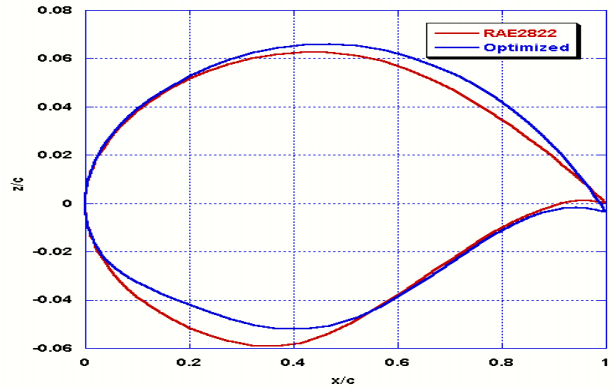

(a) Geometry of airfoils

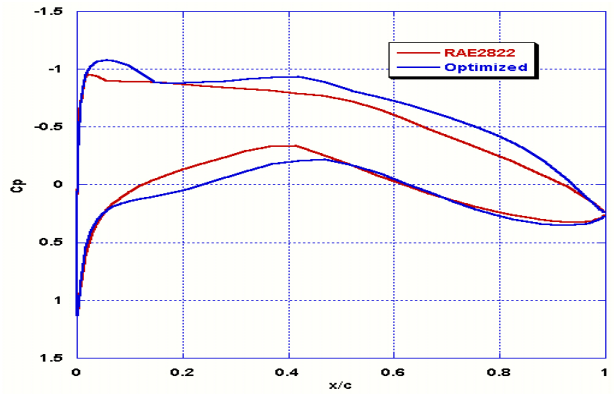

(b) Pressure distributions of airfoils

Figure 8. Comparisons of geometry and pressure distribution of airfoils

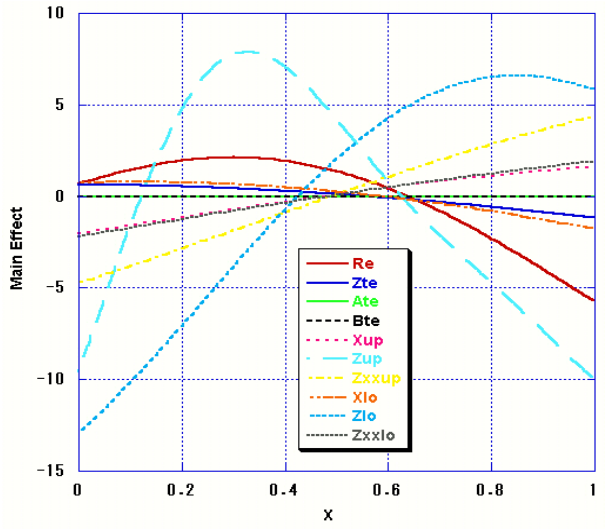

Figure 9. The main effect of design variables

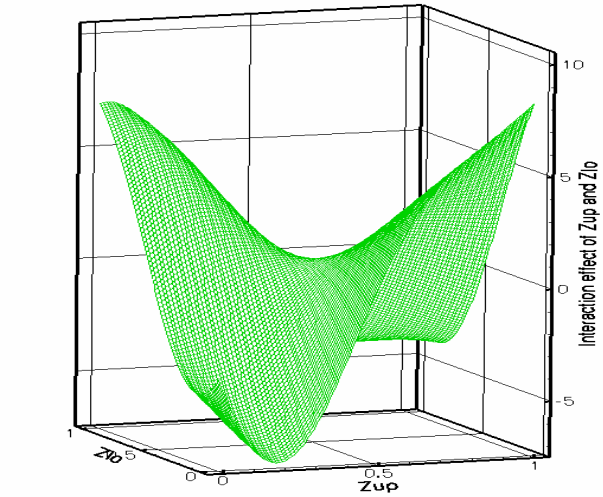

(a) Two-way interaction between Z_{UP}-Z_{LO}

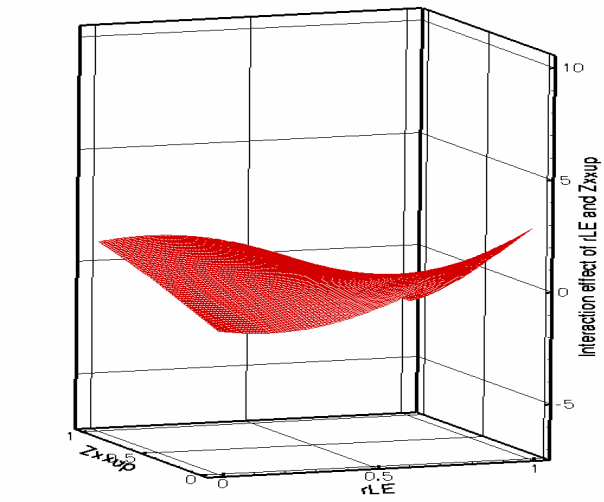

(c) Two-way interaction between r_{LE}-Z_{XXUP}

Figure 10. The two-way interaction of design variables

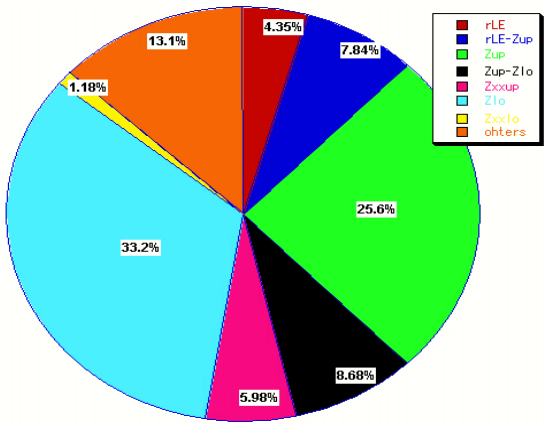

Figure 11. The proportion to the total variance

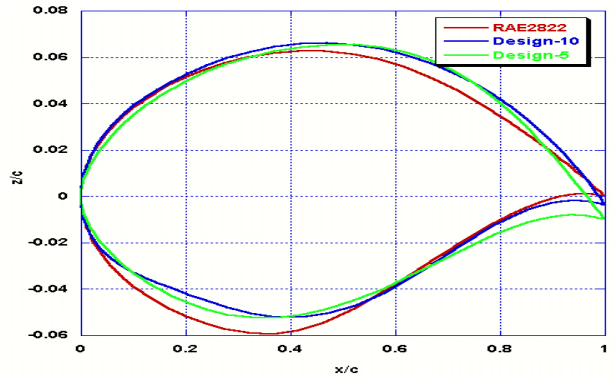

(a) Geometry

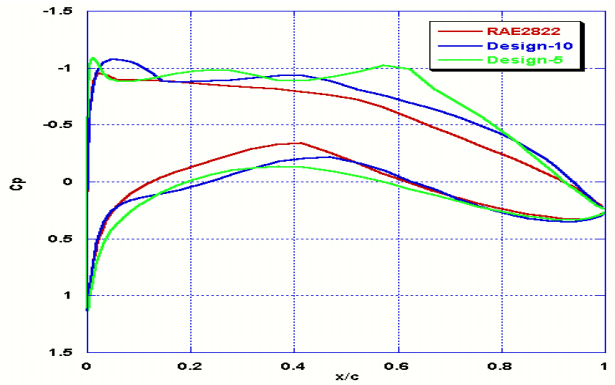

(b) Pressure distributions

Figure 12. Comparisons of geometry and pressure distribution of airfoils

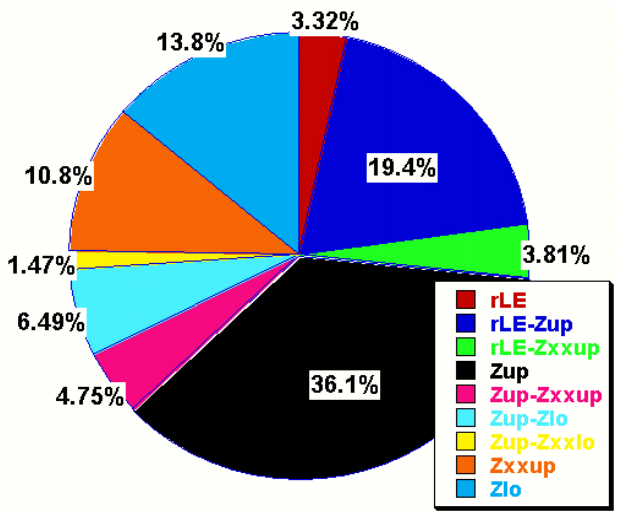

Figure 13. The proportion to the total variance

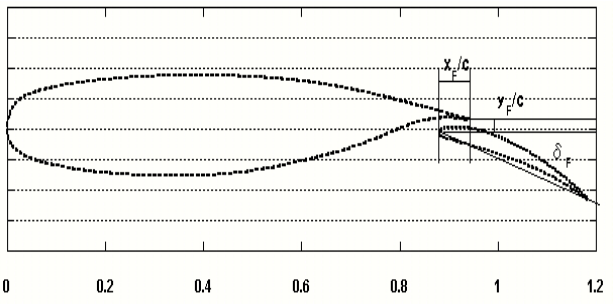

Figure 14. NLR7301 with single flap

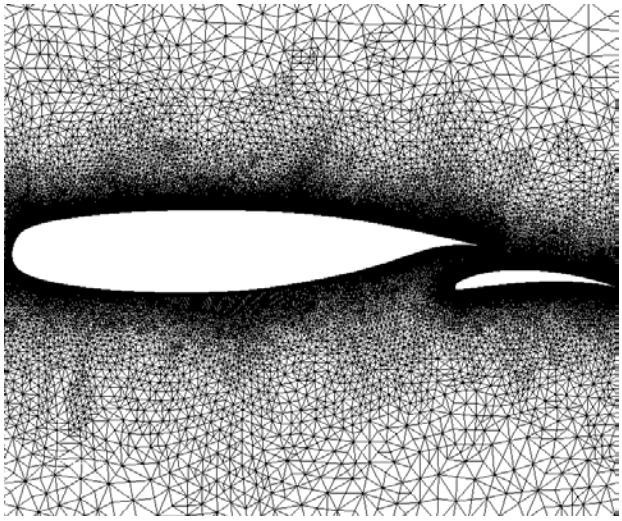

(a) Over view of computational mesh

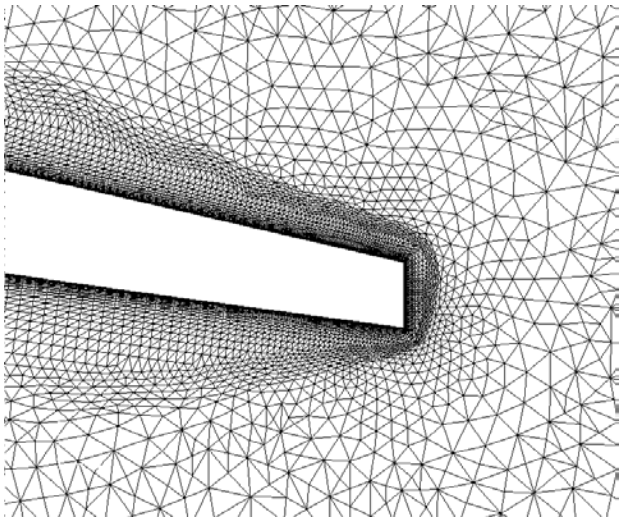

(b) Prism layer near the wall

Figure 15. Unstructured mesh around the multi elements airfoil

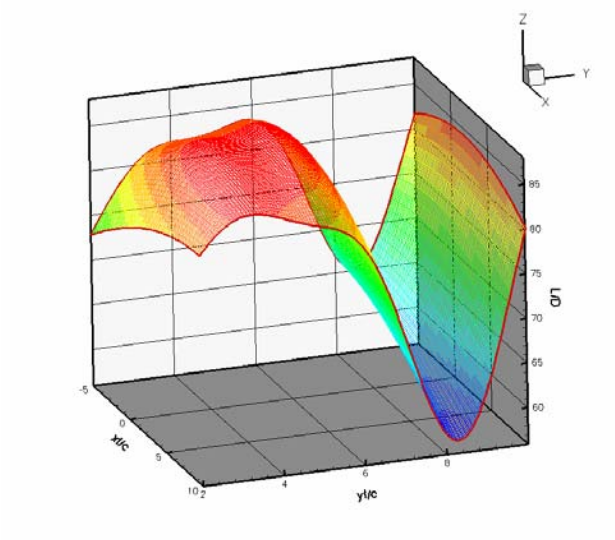

Figure 16. L/D plot at deflection angle, δ_F=9.66°